Chin. J. Astron. Astrophys. Vol. 4 (2004), No. 2, 153–165
(*http://www.chjaa.org* or *http://chjaa.bao.ac.cn*)

Chinese Journal of
Astronomy and
Astrophysics

Stellar X-ray Sources in the Rosette Nebula

Wen Ping Chen, Po-Shih Chiang and Jin-Zeng Li

Institute of Astronomy, National Central University, Chung-Li 32054, Taiwan;
wchen@astro.ncu.edu.tw
National Astronomical Observatories, Chinese Academy of Sciences, Beijing 100012

Received 2003 September 1; accepted 2003 December 2

Abstract We present optical photometric and spectroscopic studies of *ROSAT* X-ray stellar sources in the Rosette Nebula star-forming region. The brightest X-ray sources are either massive stars or active T Tauri stars associated with the open cluster NGC 2244, or are foreground stars. Some of the spectra of the young stars newly identified in the region are presented.

Key words: stars: early-type — stars: pre-main sequence — stars: formation — HII regions

1 INTRODUCTION

The Rosette Nebula is a spectacular H II region around the open cluster NGC 2244 at a distance of ∼1.67 kpc (Pérez 1991). The cluster is only ∼ 4 million years old and its OB stars are responsible for ionizing the H II region (Ogura & Ishida 1981). The Rosette Nebula appears hollow around the cluster, suggesting that fast stellar winds and radiation pressure from the hot stars in NGC 2244 have cleared away the gas and dust in the vicinity of the stars. The angular extent of the prominent emission nebula is about 1.5°, which at its distance corresponds to ∼ 40 pc.

Star formation still takes place in the Rosette Nebula and its vicinity. Localized, ionized flows associated with embedded young stellar sources, i.e., Herbig-Haro (HH) objects, have been detected in the nebula (Meaburn & Walsh 1986). A ridge of molecular gas is present to the southeast of the nebula (Blitz & Stark 1986), and seven embedded clusters have been detected in near-IR images of this molecular cloud (Phelps & Lada 1997).

X-ray observations of star forming regions like the Rosette can be used to search for diffuse emission from hot (10^6 K) gas and point sources of pre-main sequence stars. Using observations made with the imaging proportional counter of the *Einstein Observatory*, Leahy (1985) reported detection of diffuse X-ray emission from the central cavity of the Rosette Nebula, and interpreted it as shocked stellar winds. Gregorio-Hetem et al. (1998) used *ROSAT* X-ray observations of the molecular cloud southeast of the Rosette to study the star formation activity. Here we present our analysis of the *ROSAT* X-ray observations of the Rosette Nebula and its surrounding regions.

To search for diffuse X-ray emission and young stellar objects (YSOs), we have examined archival *ROSAT* observations of the Rosette. We find that the previously reported "diffuse"

X-ray emission has been largely resolved into point sources. Forty-seven point sources are detected at $\gtrsim 3\sigma$ above the background. Twenty-seven of these sources have stellar counterparts. With spectral and photometric information from the literature and new optical spectroscopic observations, we are able to distinguish coronal stars in the foreground, and OB stars and YSOs in the cluster. The YSO nature of some of these stars is further indicated by the HH-like nebular features or dust pillars in the vicinity of the stars.

This paper reports our analysis of the *ROSAT* observations of the Rosette Nebula, the point X-ray sources detected in these observations, and the identification of their optical counterparts. Section 2 describes the available *ROSAT* and optical observations of the Rosette Nebula and our method of analysis; In Section 3 we report the X-ray sources detected, their optical counterparts, and comment on the nature of these stars.

2 OBSERVATIONS AND METHOD OF ANALYSIS

2.1 X-ray Observations

The Rosette Nebula has been observed with the *ROSAT* X-ray Satellite using both the Position Sensitive Proportional Counter (PSPC) and the High Resolution Imager (HRI). The PSPC has a $\sim 2^\circ$ field of view and an on-axis angular resolution of $\sim 30''$ at 1 keV. It is sensitive to photons at the energy range of 0.1 to 2.4 keV, and has a spectral resolution of 45% at 1 keV. The HRI has a $38'$ field of view and an on-axis resolution of $\sim 5''$. It is sensitive to photons at the energy range of 0.1 to 2.0 keV, but has negligible spectral resolution.

We used the web browser provided by the High Energy Astrophysics Science Archive Research Center (HEASARC) to search for available *ROSAT* observations. Adopting a nominal center of $6^{\rm h}32^{\rm m}$, $4^\circ56'$ (J2000) for the Rosette Nebula, we have retrieved and analyzed all observations pointed within $40'$ from the nebular center. These include three PSPC observations and one HRI observation; their sequence numbers, instruments used, exposure times, dates of observation, and pointing centers are given in Table 1.

Table 1 Archival ROSAT Observations

Sequence No.	Instrument	Exposure (sec)	Dates of Observation	RA (J2000) (h m s)	Dec (J2000) (d m s)
RP200196	PSPC	4295	1992/04/02	06 31 55.02	04 56 24
RP900315	PSPC	2829	1993/04/12 – 1993/04/13	06 32 02.04	04 52 48
RP900555	PSPC	9987	1993/09/25 – 1993/10/05	06 32 07.02	04 51 36
RH202155	HRI	18799	1996/04/05 – 1996/04/11	06 31 55.02	04 56 24

The PSPC observation RP900555 ($\sim$10 ks), having the deepest exposure, provides the most extensive X-ray source list. The PSPC observations RP200196 (4.3 ks) and RP900315 (2.8 ks) detect fewer sources, but provide a longer baseline in time for identification of variable sources. The HRI observation RH202155 (18.8 ks) is useful in resolving sources in crowded regions.

2.2 Optical Emission-Line Images

Optical emission-line images of the Rosette Nebula were obtained with the 8k×8k CCD Mosaic Camera on the 0.9 m telescope at Kitt Peak National Observatory on 1999 March 2, kindly made available to us by the observer T. Rector. The pixel size is $0\farcs423$ pixel^{-1} and the field of view is roughly $1^\circ \times 1^\circ$. Images were taken with the Hα, [O III], and [S II] [O III], [S II] filters, whose central wavelengths/FWHMs are 6569/80, 5021/55, and 6730/80 in Å/Å,

respectively. The exposure time of each image was 600 s. An astrometric solution for these images was determined with the use of stars in the Guide Star Catalog 1.2 (Roser et al. 1998). The position accuracy in the optical images presented is $\sim 1''$.

2.3 Optical Spectroscopy

Low-resolution spectroscopic observations, with 200Å mm^{-1} dispersion, 4.8Å $pixel^{-1}$ and $2.5''$slit, were carried out for relatively bright sources ($m_V < 14$ mag) by the 2.16 m telescope at Xinglong of the National Astronomical Observatory of China, during 16–25 December 2000, and again during 9–12 October 2001. A Tek1024 CCD detector was used. The results for some bright sources observed in 2000 have been reported by Li et al. (2002), in which a couple of Herbig Ae/Be stars and possible weak-lined T Tauri stars were identified. The instrumentation setup and data reduction procedures for the 2001 run were the same as those for the 2000 run reported in Li et al. (2002).

2.4 Method of Analysis

To examine the PSPC observations, we extracted images from the event files, binning the data spatially by a factor of 10 to $5''$ pixels and collapsing the energy bins into the 0.1–2.4 keV band. The resultant images were smoothed by a Gaussian with $\sigma = 2$ pixels ($10''$) to improve the S/N ratio. The HRI observation was binned by a factor of 2 to obtain $1''$ pixels and smoothed by a Gaussian with $\sigma = 3$ pixels ($3''$). The smoothed images of the deepest PSPC (RP900555) and the HRI observations are presented in Fig. 1. These smoothed images were visually examined for point sources, and the event files were used to measure the counts detected at the sources and the surrounding background regions. Whenever a source is detected in one of the four *ROSAT* observations, the other three observations are examined and the source is measured. The results show that the easily identified sources all have $> 3\sigma$ detections, while the possible-but-uncertain sources have $2 < \mathrm{S/N} < 3$. The X-ray sources are listed in Table 2. We have compared our sample of visually selected sources to those in the WGACAT, a catalog of point sources detected by the *ROSAT/PSPC* generated by an automated algorithm. We find that the difference between the two samples lies mostly in sources identified at the $\sim 2\sigma$ level in the WGACAT.

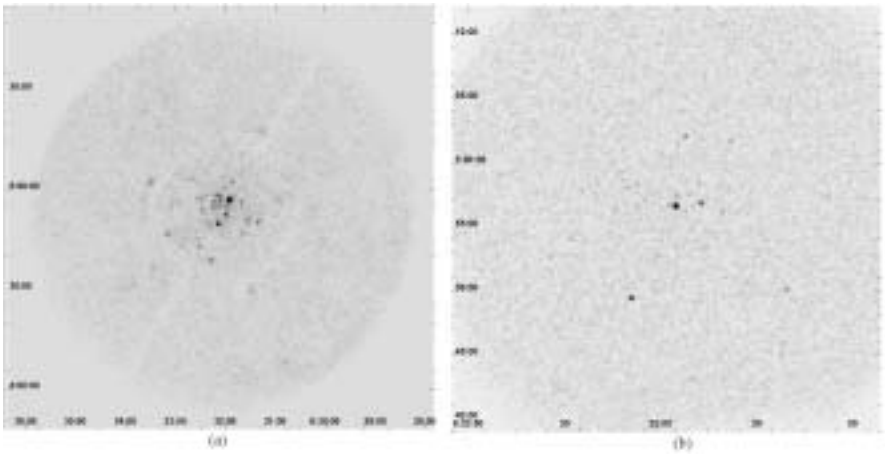

Fig. 1 Greyscale image of (a) the deepest ROSAT PSPC observation (RP900555) and (b) the ROSAT HRI observation of the Rosette Nebula.

Table 2 X-ray Sources in the Rosette Nebula

No.	Source Name RXJ	α(J2000) h m s	δ(J2000) d m s	Background-subtracted Count Rate (counts ks^{-1}) RP900555	RH202155	RP200196	RP900315
1	0631.2+0517	06 31 15.8	05 17 22	8.50 ±1.74			
2	0631.3+0450	06 31 20.7	04 50 02	5.14 ±0.91	2.77 ±0.63	3.51 ±1.42	
3	0631.5+0429	06 31 30.6	04 29 31	11.03 ±1.96			
4	0631.5+0450	06 31 33.3	04 50 38	3.67 ±0.80			
5	0631.6+0446	06 31 40.6	04 46 38	2.64 ±0.73			
6	0631.6+0456	06 31 41.0	04 56 09	4.98 ±0.88	1.51 ±0.57	4.68 ±1.53	
7	0631.7+0456	06 31 47.4	04 56 51		4.79 ±0.72	3.05 ±1.37	
8	0631.8+0453	06 31 48.4	04 53 26	1.56 ±0.61		5.60 ±1.61	
9	0631.8+0458	06 31 48.6	04 58 19	1.78 ±0.63			
10	0631.8+0451	06 31 51.8	04 51 18	1.99 ±0.65			
11	0631.8+0502	06 31 52.5	05 02 03	4.64 ±0.90	2.03 ±0.59	5.13 ±1.57	
12[a]	0631.9+0457	06 31 54.9	04 57 21		2.19 ±0.61		
13[a]	0631.9+0456	06 31 55.4	04 56 37	43.99 ±2.29	17.57 ±1.11	40.06 ±3.38	37.02 ±4.02
14[e]	0631.9+0453	06 31 56.7	04 53 56			6.99 ±1.72	
15[a]	0631.9+0456	06 31 57.4	04 56 45		1.61 ±0.56		
16	0631.9+0455	06 31 59.4	04 55 33	2.64 ±0.71			
17	0632.0+0452	06 32 00.0	04 52 18	7.74 ±1.05			
18	0632.0+0500	06 32 00.4	05 00 53	2.25 ±0.68			
19	0632.0+0452	06 32 00.6	04 52 39		1.76 ±0.58		
20	0632.0+0503	06 32 02.0	05 03 18	2.13 ±0.69			
21[b]	0632.0+0457	06 32 04.7	04 57 59	1.65 ±0.64		8.86 ±1.86	7.38 ±2.08
22[b]	0632.1+0457	06 32 06.0	04 57 05	4.10 ±0.85			7.32 ±2.08
23	0632.1+0455	06 32 07.0	04 55 28	2.93 ±0.76			
24	0632.1+0456	06 32 07.2	04 56 33	3.67 ±0.82	1.34 ±0.56	2.81 ±1.35	
25	0632.1+0458	06 32 07.7	04 58 13	3.14 ±0.78		3.51 ±1.42	
26	0632.1+0449	06 32 09.2	04 49 27	18.29 ±1.53	7.67 ±0.82	15.37 ±2.27	23.58 ±3.31
27	0632.1+0454	06 32 10.1	04 54 28	2.50 ±0.72		3.51 ±1.42	
28	0632.1+0458	06 32 10.3	04 58 03	4.63 ±0.88	1.50 ±0.57		
29	0632.2+0453	06 32 12.4	04 53 58	1.97 ±0.67			
30[c]	0632.2+0456	06 32 14.2	04 56 29	3.88 ±0.83	1.29 ±0.56	6.30 ±1.67	5.20 ±1.84
31	0632.2+0454	06 32 16.1	04 54 23	3.14 ±0.78			4.14 ±1.71
32	0632.2+0455	06 32 16.6	04 55 21	2.31 ±0.68			
33	0632.3+0438	06 32 18.1	04 38 33	4.32 ±0.88		3.28 ±1.39	3.44 ±1.62
34	0632.3+0448	06 32 20.1	04 48 13	2.20 ±0.67			
35	0632.3+0449	06 32 23.3	04 49 34	1.78 ±0.63			
36	0632.4+0457	06 32 25.6	04 57 42	2.10 ±0.66			
37	0632.4+0455	06 32 26.2	04 55 34	1.88 ±0.64			
38	0632.4+0454	06 32 28.5	04 54 13	3.07 ±0.76	1.39 ±0.56	4.43 ±1.51	
39	0632.4+0456	06 32 29.8	04 56 58	3.28 ±0.77			
40	0632.5+0442	06 32 31.5	04 42 33	4.53 ±0.88			
41	0632.5+0457	06 32 32.5	04 57 18	2.68 ±0.71			
42	0632.6+0502	06 32 39.1	05 02 46	1.85 ±0.68			
43	0632.7+0502	06 32 44.2	04 48 01	1.66 ±0.65			
44	0633.0+0454	06 33 05.6	04 54 53	2.76 ±0.88		6.06 ±1.65	
45[d]	0633.1+0446	06 33 08.6	04 46 28	9.56 ±1.41			4.85 ±1.79
46	0633.4+0436	06 33 26.7	04 36 17	6.27 ±1.51			
47	0633.5+0502	06 33 30.5	05 02 00	15.72 ±2.10			

[a] Near a bright source; hard to identify beside HRI observation;
[b] Diffuse region. In RP200196 and RP900315, sources 21 and 22 are merged together;
[c] Candidate of Herbig-Haro object;
[d] Pillar object;
[e] Not well-defined point source.

To identify optical counterparts of the X-ray sources, the contours of the smoothed PSPC observation RP900555 are plotted over the Hα image (Fig. 2). For easy viewing of visible

stars within the PSPC point-spread-function, the X-ray sources listed in Table 2 are plotted as circles, with sizes appropriate for the off-axis angles, over the Hα image (Fig. 3). For example, the circles have radii of $8''$, $16''$, and $24''$ for off-axis angles of $\leq 10'$, $15'$, and $20'$, respectively. Figure 4 plots separately the X-ray sources in the central, crowded region.

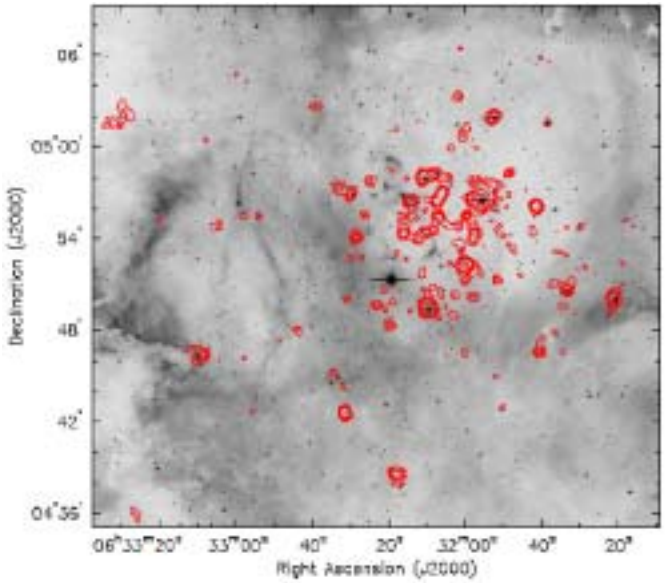

Fig. 2 H-alpha image of the Rosette Nebula made with the KPNO/MOSAIC imager overlaid with contours to show the ROSAT PSPC emission. Contour levels are at 0.02, 0.03, 0.04, 0.10, 0.30, 0.90 cts ks^{-1}.

The cluster NGC 2244 in the Rosette Nebula has been extensively studied. UBV photometry of stars in NGC 2244 has been reported by Ogura & Ishida (1981, hereafter OI), Massey, Johnson& DeGioia-Eastwood (1995) (hereafter MJD), Park & Sung (2002), and Berghöfer & Christian (2002). Available spectral classification of stars in NGC 2244 has been compiled by Ogura & Ishida (1981). Additional spectral classification observations have been reported by Pérez, Thé & Westerlund (1987) and by MJD (1995). Less reliable spectral types of NGC 2244 stars have been derived by the photometry of Kuznetsov et al. (2000) using Ogura & Ishida (1981). Table 3 lists the reliable spectral classification of stars in NGC 2244. We have used these spectral types and photometry data from the literature to determine the properties of the stars.

For stars that do not have spectral classifications, different combinations of photometric data may provide useful diagnostics for their spectral types. We have used MJD's UBV photometry to construct the color-magnitude diagram of V vs $(B-V)$ and the color-color diagram of $(U-B)$ vs $(B-V)$. In addition, we have followed Ogura & Ishida (1981) and made an extinction-free P-Q color-magnitude diagram, where $P \equiv V - (A_V/E(B-V))\,(B-V)$ is effectively an extinction-free magnitude and $Q \equiv (U-B) - (E(U-B)/E(B-V))\,(B-V)$ is a reddening-free color index. In this paper we adopt $A_V/E(B-V) = 3.1$ and $E(U-B)/E(B-V) = 0.72$ (Ogura & Ishida 1981). These diagrams are presented as Figs. 5 and 6, respectively. For comparison, a main sequence is plotted in the color-color diagram, and a main sequence at the distance of NGC 2244 is plotted in the color-magnitude diagrams. The extinction-free color-magnitude

diagram (P vs Q), while not widely known, is very useful in judging whether a star is foreground or background to the cluster NGC 2244.

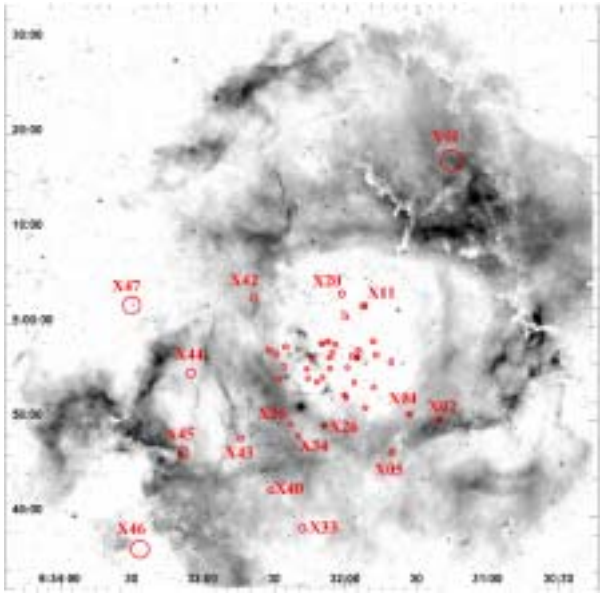

Fig. 3 H-alpha image of the Rosette Nebula made with the KPNO/MOSAIC imager overlaid with X-ray sources detected by ROSAT. The size of each circle approximates the precision with which the X-ray source position could be measured (i.e. $\sim 8''$ for R$\leq 10'$, $\sim 16''$ for R$=15'$, and $\sim 24''$ for R$=20'$, where R is the angular offset from the optical axis of the ROSAT PSPC.)

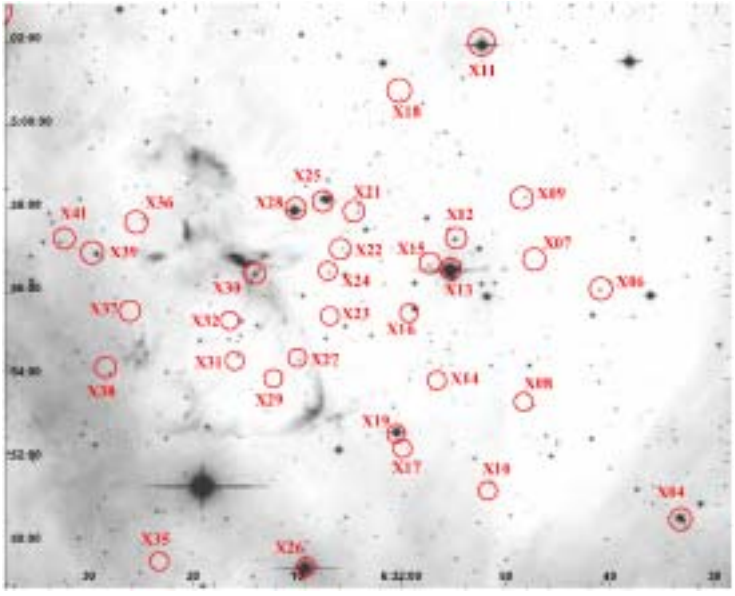

Fig. 4 Same as Fig. 3 but for the crowded region at the center of the Rosette Nebula.

Table 3 Stellar Counterparts of X-ray Sources in the Rosette Nebula

X-ray No.	Pos. Err. [']	Star Offset [']	Optical Identification	V [mag]	$(B-V)$ [mag]	$(U-B)$ [mag]	Spec. Type	HD/HDE	Comments
1	65		J063115.70+051724.7 (B 13)	14.27	0.81				
2	20	3	J063120.88+045004.0 (M454)	8.22	0.15	−0.73	O8 V((f))	46056	M
3	54	17	J063129.52+042935.2 (M201)	9.45	0.74	0.26	G0[d]	258987	F
4	16	3	J063133.13+045035.9 (M203)	12.45	0.36	−0.18			M
		3	J063133.48+045040.0 (M533)	9.39	0.14	−0.64	B1 V	259012	M
5	16		J063141.50+044640.3 (B 28)	17.76					
6	16	2	J063141.12+045607.8 (M347)	14.09	1.12	0.37			F
7	16		J063147.70+045649.9 (B 36)	18.08					
8	13		J063147.80+045316.3 (B 38)	15.96	1.21				
			J063148.10+045338.0 (P124)	16.11	1.34	1.01			F
9[1]	16		J063148.30+045820.5 (B 39)	15.95	1.28				
			J063148.30+045820.0 (P125)	16.77	1.25	0.62			F
			J063148.30+045821.0 (P126)	16.52	1.67	0.54			?
10	13		J063151.60+045124.2 (B 43)	16.88	1.48				
11	19	4	J063152.54+050159.4 (M713)	7.72	0.18	−0.61	O8. 5 V((f))	46149	M
12	15	4	J063155.12+045719.6 (M360)	12.35	0.33	−0.26			M
13	15	3	J063155.53+045634.5 (M354)	6.87	0.12	−0.85	O5 V((f))[d]	46150	M
14	13								
15	15	4	J063158.00+045637.4 (B 55)	17.95B					
			J063157.50+045642.0 (P205)	14.89	1.39	1.00			F
16	13	10	J063158.95+045540.1 (M410)	10.36	0.21	−0.54	B1 .5 V		M
17	13								
18	17		J063200.30+050042.0 (B 58)	16.34	1.39				
			J063200.30+050042.0 (P222)	16.19	1.44	0.98			F
19	13	2	J063200.62+045241.1 (M382)	8.54	0.14	−0.70	B0. 5 Vdbl	259135	M
20	20		J063202.20+050319.3 (B 66)	16.51	0.99				
			J063202.20+050320.0 (P237)	16.42	1.29	0.85			F
21[2]	15	5	J063204.38+045758.7 (M505)	15.26	0.94	0.11			F?
			J063204.90+045748.9 (B 73)	17.31	0.92				
			J063204.40+045758.0 (P251)	15.20	1.02	0.46			F
			J063204.40+045759.0 (P252)	16.98	0.82	0.65			F
22	15		J063205.40+045659.3 (B 77)	15.69	1.32				
			J063205.40+045700.0 (P258)	15.68	1.39	1.00			F
			J063205.90+045706.0 (P264)	16.55	1.51				
23	13		J063206.70+045530.6 (B 78)	17.22	1.40				
24	13	4	J063207.10+045629.8 (B 79)	14.59	1.09				
			J063207.10+045630.0 (P277)	14.45	1.26	0.75			F
25	15	4	J063207.69+045817.0 (M151)	10.34	0.31	−0.02			F
		6	J063207.35+045816.3 (M400)	8.80	0.09	0.02	A3 V[d]	46180	F
26	13	3	J063209.32+044924.9 (M394)	7.27	0.21	−0.78	O4 V((f))	46223	M
27	13		J063210.00+045423.2 (B 85)	15.48	1.17				
			J063210.00+045423.0 (P301)	15.43	1.22	0.66			F
28	15	4	J063210.48+045800.1 (M370)	8.21	0.14	−0.67	O9 V((f))	46202	M
29	13		J063211.60+045357.0 (P308)	15.84	1.33	0.92			F
30	15	2	J063214.21+045627.4 (M374)	11.23	0.23	0.08		259210	F
			J063214.50+045618.0 (P321)	13.81	0.70	0.16			M
31	13	8	J063215.85+045430.2 (M 47)	14.57	1.09	0.84			F
32	13		J063215.50+045520.3 (B 90)	12.00	0.37				
			J063215.50+045521.0 (P327)	12.01	0.32	−0.25			M
			J063216.20+045530.0 (P334)	16.85	1.43				
33	22	5	J063217.88+043829.0 (M157)	13.34	0.80	0.13			F
34	13	7	J063219.95+044819.2 (M181)	14.40	1.19	0.50			F
35	13		J063223.10+044943.1 (B101)	17.92	—				
36	16		J063224.86+045746.7 (M 95)	14.35	0.84	0.29			F
37	15		J063224.90+045536.2 (B105)	17.78I					
38	15		J063228.10+045403.6 (B108)	14.66	1.03				
			J063228.10+045404.0 (P429)	14.57	1.09	0.45			F
39	16	6	J063229.40+045656.3 (M405)	10.78	0.30	−0.29	B3 V p[d]	259300	M
40	19	1	J063231.46+044234.1 (M283)	14.56	1.36	0.89			F
41	15	8	J063232.88+045712.7 (M369)	14.38	0.64	0.14			F
42	22	4	J063239.17+050249.8 (M617)	14.93	0.73	0.34			F
43	17	3	J063244.12+044758.1 (M298)	15.57	1.25	0.52			F
44	27	13	J063305.14+045442.3 (M445)	13.68	0.87	0.24			F
45	32	16	J063309.61+044624.5 (M476)	12.94	1.20	0.56			F
46	56		J063327.50+043556.6 (B136)	13.90	0.79				
47	54	7	J063330.10+050203.3 (M671)	9.74	0.79	0.23		259635	F

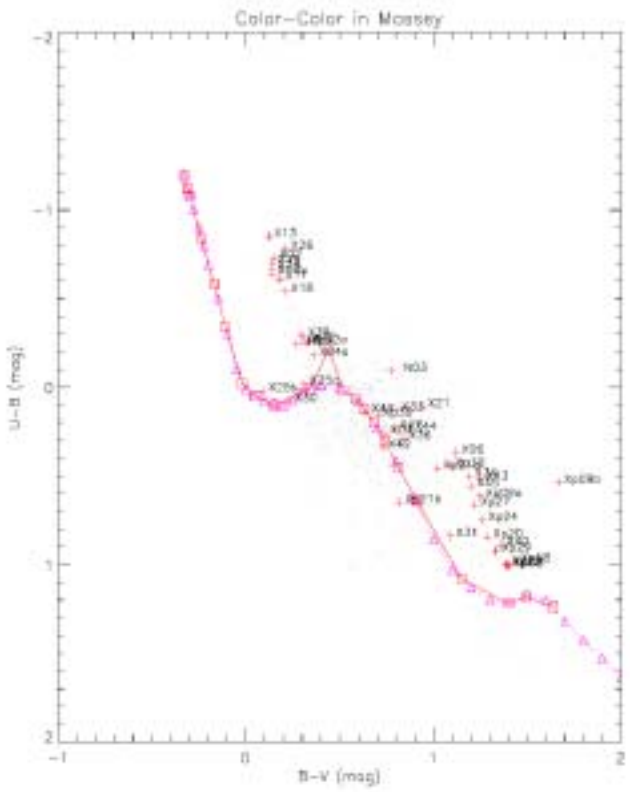

Fig. 5 Color-color $(U-B)$ versus $(B-V)$ diagram for the sources detected by MJD (1995). Approximate location of the unreddened main sequence and ZAMS are overlaid using canonical values from Schmidt-Kaler (1982).

3 X-RAY SOURCES AND OPTICAL COUNTERPARTS

Stellar counterparts of the X-ray sources can be seen in Fig. 3 and Fig. 4. Table 3 summarizes the results: (1) the X-ray source number, (2) the off-axis angle of the source in the field-of-view of RP900555, (3) the actual positional offset between the X-ray source and the optical counterpart, (4) the optical identification of the stellar counterpart, with the reference (M: MJD (1995), P: Park & Sung (2002), B: Berghöfer & Christian (2002)) and the corresponding sequential number, (5) V magnitude, (6) $(B-V)$, (7) $(U-B)$, (8) spectral type, (9) HD or HDE catalog number, and (10) comments. In the course of this study, Berghöfer & Christian (2002) published their results on the *ROSAT* data of NGC 2244 in the Rosette Nebula. They used the same *ROSAT* archival data as we did, and performed broadband photometry of optical counterparts to X-ray sources. However, we processed the *ROSAT* data differently and included spectral information in our study. Some of the optical identifications in Berghöfer & Christian (2002) have been incorporated in Table 3.

It is immediately clear from Table 3 that the brightest ($V < 10$ mag) optical counterparts of the X-ray sources are mostly early-type stars in NGC 2244 or late-type foreground stars. Some faint optical counterparts of the X-ray sources may have been included in the photometric

observations of Ogura & Ishida (1981) and MJD (1995) but without spectral classifications. Still fainter optical counterparts are not included in any photometric studies, and the faintest sources are not even visible. These different types of stellar sources are further discussed below.

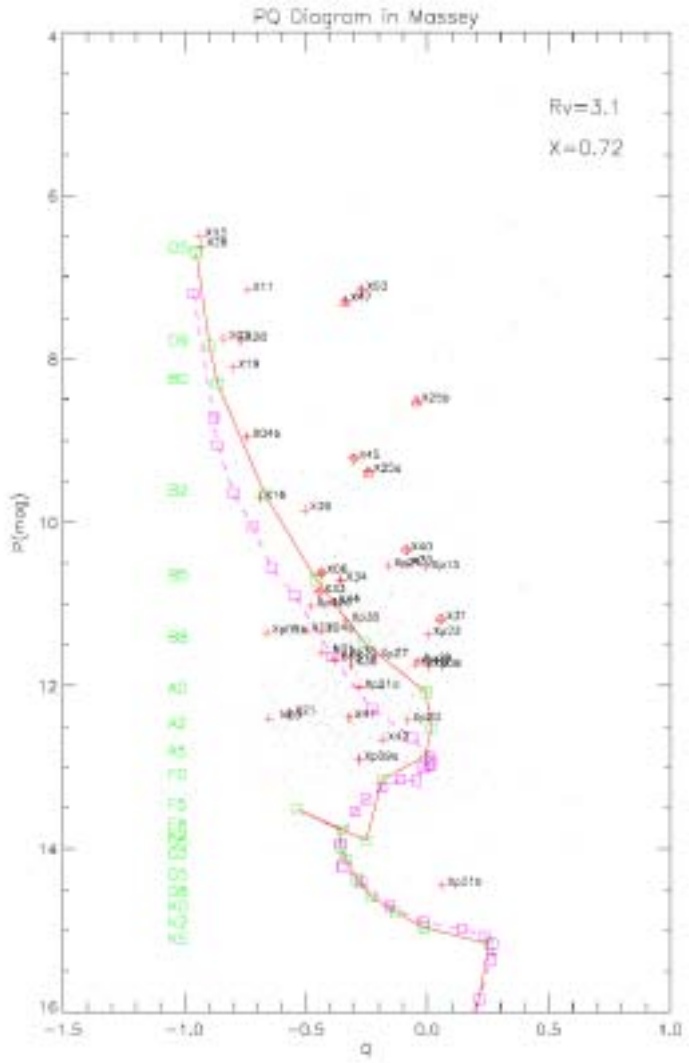

Fig. 6 Plot of the reddening-free indices P and Q for the sources detected by MJD (1995). Approximate location of the corresponding main sequence and ZAMS are overlaid using canonical values from Schmidt-Kaler (1982). Note that because the indices P and Q are reddening free, the main sequence and ZAMS are properly plotted for the distance to NGC 2244.

3.1 Young Stellar Population

Pre-main sequence (PMS) stars are known to be with X-ray emission due to instability-driven energetic winds from massive stars, or chromospheric/coronal magnetic activity in low-mass stars. In nearby molecular complexes (e.g., Taurus, Ophiuchus, Lupus, Corona Australis,

Chamaeleon, all about 150 pc) X-ray emission has been detected from young stars at different evolutionary stages, from mass accreting T Tauri phase, to isolated weak-lined T Tauri phase. Protostars embedded in clouds are also found to be X-ray emitters, especially in the hard X rays where interstellar and circumstellar extinction becomes noticeably small (Feigelson & Montmerle 1999).

Using the four *ROSAT* observations of the Rosette Nebula, we have identified 47 point sources, of which 40 are detected at $> 3\sigma$ level and 7 at 2.5–3 σ level (see Table 2). While most of the sources are detected in the longest PSPC observation (RP900555), some sources are detected in the shorter exposures but not in the longest one, indicating that these latter sources must be X-ray variables, common among PMS objects with typical time scales of hours (flares) to days (Feigelson & Montmerle 1999). Source No. 7 has the most secured X-ray variability identification because it is detected in both PSPC short exposures and the HRI image, but not in the longest exposure.

Figure 7 plots the positions of X-ray (*ROSAT*) sources and far-infrared (*IRAS*) sources in the Rosette. The spatial distributions are quiet different from each other. The *ROSAT* sources appear mostly in the central cavity of the Rosette Nebula, for which data are available. In contrast the *IRAS* sources are found throughout the whole region, and in general do not coincide with X-ray sources. It is likely that the *IRAS* detected a wide family of embedded objects, in some cases associated with giant nebulous pillars, while *ROSAT* was sensitive only to the brightest X-ray sources, which at 1.6 kpc turn out to be the OB stars at the center of the nebula.

Our sources typically have been detected with a few counts per kilosecond, too low to do spectral analysis. Given a ∼1.5 mag extinction toward these sources, as estimated from the averaged color excess, $E(B-V)$ ∼0.48–0.54 (Pérez 1991; Yadav & Sagar 2001), the X-ray luminosity of our sources amounts to $L_{\rm x} \gtrsim 7 \times 10^{30}$ erg s^{-1}. This is to be compared with the X-ray luminosity of typical T Tauri stars, $L_{\rm x} \sim 10^{28.5}$ to 10^{31} erg s^{-1} in their quiescent states (Feigelson & Montmerle 1999). Because the Rosette is some ten times more distant than nearby molecular clouds, only the brightest T Tauri X-ray-emitters, or those which happened to undergo flaring events, could have been detected by *ROSAT*.

The bright X-ray sources in our sample are either early-type member stars or late-type field stars. The brightest X-ray sources, No. 13 and 26, coincide in positions with the earliest types of stars in the region, O5 and O4, respectively. Other X-ray bright sources, No. 1, 3 and 47 are foreground stars (see below). Berghöfer et al. (1997) found that X-ray stars with spectral types earlier than ∼B1.5 are soft X-ray emitters, with a ratio of X-ray to bolometric luminosity $L_{\rm x}/L_{\rm bol} \sim 10^{-7}$. The strongest X-ray sources in our sample, No. 13, has a PSPC detection of ∼ 44 counts per kiloseconds which, adopting a conversion factor of 0.41×10^{11} ct cm^{-2} erg, gives $L_{\rm x} \sim 5.2 \times 10^{31}$ erg s^{-1}. This O5 V star is also the brightest visible star in our sample, with $m_V = 6.87$ and $(B-V)$=0.12 (MJD). Given an absolute magnitude $M_V = -5.7$, a bolometric correction of –4.40, and $(B-V)$ color of –0.33 for an O5 V star (Cox 2000), data of No. 13 are consistent with being a cluster member at a distance of ∼ 1.6 kpc, with $L_{\rm bol} \sim 8.6 \times 10^5 L_\odot$. This gives $L_{\rm x}/L_{\rm bol} \sim 10^{-7}$, well within the canonical range for massive stars.

The spectrum of the X-ray star No. 9 (Fig. 8) shows both H_α emission and the Li I 6708 Å absorption line, indicative of its youth. Its shape is elongated in the KPNO images, suggesting a binary nature, reported already by Park & Sung (2002). No. 9 therefore is a young binary system.

Source No. 30 is in a complex nebulous region with high-speed knots (Meaburn & Walsh

1986). Two stars are clearly identified within its positional error. Combination of the PQ diagram and the color-color diagram suggests that one may be a late B-type member star, while the other a foreground star.

Source No. 45 is bright in X rays and has an optical counterpart near a nebular pillar. Its spectrum shows possible presence of Li I 6708 absorption (see Fig. 8). Recent *Chandra* data show a point source at the position of the optical star. The optical KPNO images and the *Chandra* image suggest existence of shocked gas near the apex of the pillar. It is possible that the shocked gas is caused by the optical star.

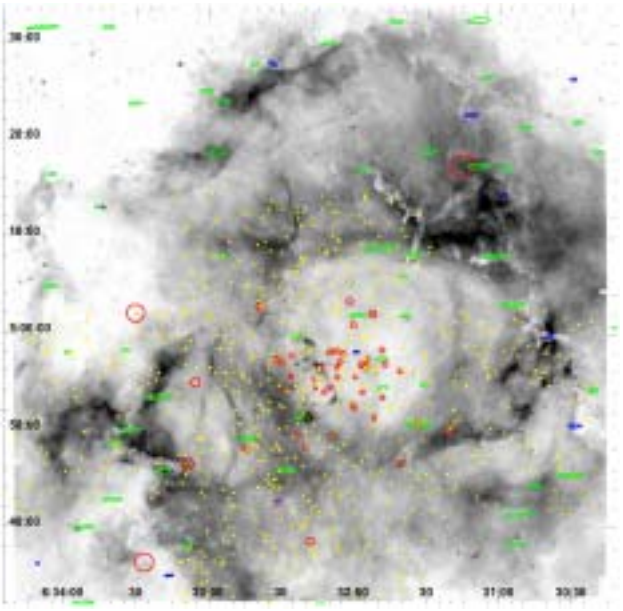

Fig. 7 *ROSAT* X-ray sources (circles) and *IRAS* infrared sources (ellipses) in the Rosette Nebula. The ellipse for each *IRAS* source corresponds to its positional errors.

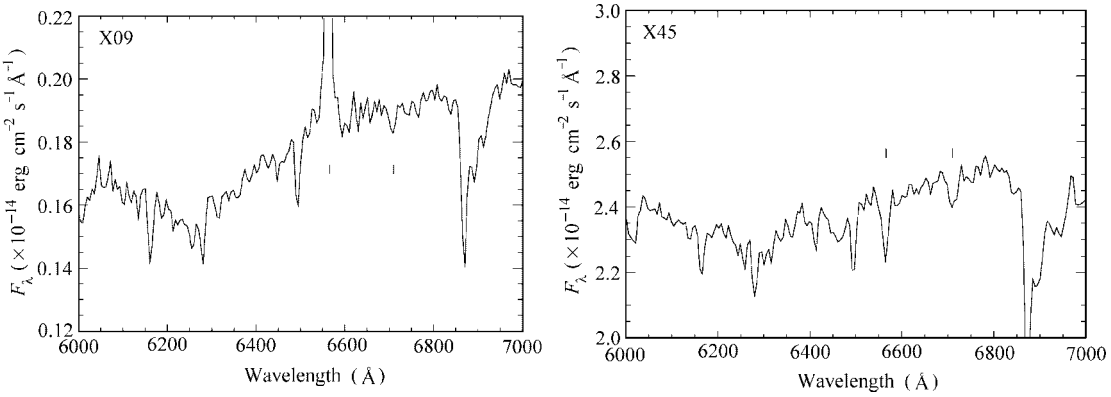

Fig. 8 Spectra of No. 9 and No. 45. The H_α and Li I 6708 Å lines are marked.

The star 063129.8+045449 is a slightly less than $\sim 2\sigma$ *ROSAT* detection, thus not included in Table 2. It was first reported by Chiang & Chen (2001) as a source associated with strong H_α emission nebulosity, and later discussed in detail by Li et al. (2002) as a possible Herbig Ae star. Associated with the star is a faint nebula seen to the south. The presence of prominent H_α and [S II], together with the absence/weakness of the [O III] emission, suggests that the nebulosity may be a Herbig-Haro object.

A serendipitous finding on the optical images is the star 063220.8+045303 which appears to be associated with a jet (Fig. 9). It was not detected by *ROSAT*, but was detected by recent *Chandra* observations. Its spectrum shows an early-type star with strong H_α and nebular [O III]. Notably, it is seen associated with a jet in the H_α and [S II] images, but the jet-like structure is not as prominent in the [O III] image.

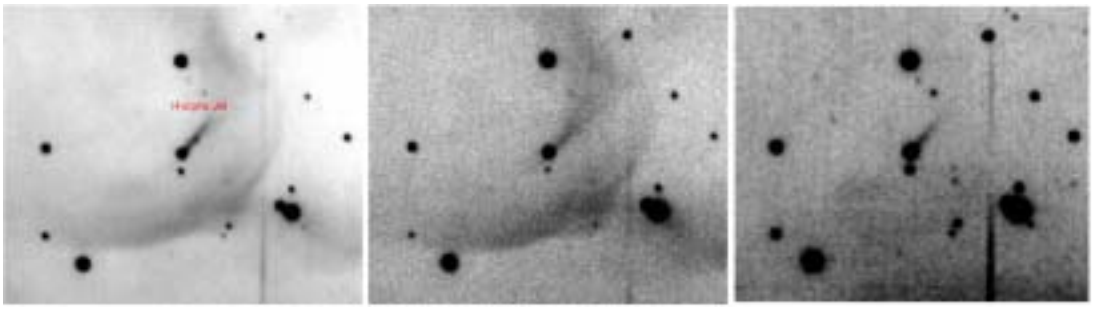

Fig. 9 Images of 063220.8 + 045303 in, left to right, H_α, O III, and S II.

3.2 Foreground Stars

Some X-ray sources are foreground stars. The X-ray source No. 3 is associated with OI 382, classified as a G0 star in the SAO catalog. Its colors and magnitudes are consistent with a G0 V star and (with A_V ~0.51 mag) at a distance of 80 pc. The optical star for source No. 47, OI 393 does not have a spectral classification available, but its colors and magnitudes suggest a G0 V star at a distance of 86 pc with an A_V of 0.67 mag.

Within the error circle of the X-ray source No. 25, there are two candidate optical counterparts, No. 178 and No. 179 in Ogura & Ishida (1981). The foreground A3 V star OI 178 is not as close to the X-ray source position as OI 179; hence OI 179 is more likely to be the optical counterpart. The colors and magnitudes of OI 179 suggest it to be an early F type foreground star.

About half of the 47 X-ray sources in our sample are found to be foreground stars on the basis of their colors and magnitudes. This is consistent with the *ROSAT* PSPC source density toward this direction of the Galaxy (Sciortino et al. 1998).

In summary, we have found young stars in the Rosette Nebula by identifying optical counterparts of X-ray sources, and by confirming their youth nature with optical photometric and spectroscopic studies. Two Herbig Ae/Be stars, as weak X-ray sources, have been identified, as direct evidence that star formation activity is going on in the region. The Rosette Nebula is therefore a good laboratory to study star formation, star-ISM interaction, and formation of star clusters. A combination of the PQ and color-color diagrams proves a useful tool to determine membership of stellar clusters, as verified by followup spectroscopic observations. Our study indicates that *ROSAT* could detect only the OB stars, and the brightest or active T Tauri

stars at the distance to the Rosette Nebula. Late-type stars associated with X-ray sources are foreground stars. Five of these show possible Li absorption. Recent observations by *Chandra*, with its improved sensitivity, would be valuable to study the low-mass young stellar population in this region.

Acknowledgements We thank Y. H. Chu and R. Grundl for assistance in processing the *ROSAT* data and in drafting the early version of this manuscript. Gratitude also goes to T. Rector for providing the H-alpha image of the Rosette Nebula, and to the referee Prof. J. Y. Hu for critical comments. This research is financially supported by grants NSC92-2112-M-008-047, and NSC92-2112-M-008-048.

References

Berghöfer T. W., Schmitt J. H. M. M., Danner R., Cassinelli J. P., 1997, A&A, 322, 167
Berghöfer T. W., Christian D. J., 2002, A&A, 384, 890
Blitz L., Stark A. A., 1986, ApJ, 300, L89
Clayton C. A., Meaburn J., 1995, A&A, 302, 202
Clayton C. A., Meaburn J., Lopez J. A., Christopoulou P. E., Goudis C. D., 1998, A&A, 334, 264
Chiang P. S., Chen W. P., 2001, In: Chen W. P., Lemme C., Paczyński B. eds., IAU Colloq. 183, Small-Telescope Astronomy on Global Scales (ASP Conf. Series, v. 246), p.335
Corporon P., Lagrange A.-M. 1999, A&AS, 136, 429
Cox A. N., 2000, Allen's Astrophysical Quantities, 4th ed., New York: AIP
Cox P., Deharveng L., Leene A., 1990, A&A, 230, 181
Feigelson E. D., Montmerle T., 1999, ARA&A, 37, 363
Gregorio-Hetem J., Montmerle T., Casanova S., Feigelson E. D., 1998, A&A, 331, 193
Flaccomio E., Micela G., Sciortino S., Damiani F., Favata F., Harden F. R., Jr, Schachter J., 2000, A&A, 355, 651
Kuznetsov V. I., Boutenko G. Z., Lazorenko G. A., Lazorenko P. F., 2000, A&AS, 142, 389
Leahy D. A., 1985, MNRAS, 217, 69
Li J. Z. et al., 2002, AJ, 123, 2590
Massey P., Johnson K. E., DeGioia-Eastwood K., 1995, ApJ, 454, 151 (MJD)
Meaburn J., Walsh J. R., 1986, MNRAS, 220, 745
Ogura K., Ishida K., 1981, PASJ, 33, 149 (OI)
Park B.-G., Sung H., 2002, AJ, 123, 892
Pérez M. R., 1991, RMxAA, 22, 99
Pérez M. R., Thé P. S., Westerlund B. E., 1987, PASP, 99, 1050
Phelps R. L., Lada E. A., 1997, ApJ, 477, 176
Roser S., Morrison J. E., Bucciarelli B., Lasker B., McLean B. J., 1998, In: B. J. McLean, D. A. Golombek, J. J. E. Hayes, H. E. Payne, eds., IAU Symposium 179, New Horizons from Multi-wavelength Sky Surveys, Dordrecht: Kluwer, 420
Schmidt-Kaler Th. 1982, Landolt-Börnstein: Numerical Data and Funtional Relationships in Science and Technology, K. Schaifers, H. H. Voigt, eds., Berlin: Springer-Verlag, VI/2b
Sciortino S., Damiani F., Favata F., Micela G., Pye J., 1998, Astron. Nachr., 319, 108
Waters L. B. F. M., Waelkens C., 1998, ARA&A, 36, 233
Yadav R. K. S., Sagar R., 2001, MNRAS, 328, 370